A&A 383, 558–567 (2002)
DOI: 10.1051/0004-6361:20011746

Astronomy & Astrophysics

The spectroscopic binaries 21 Her and γ Gem*

H. Lehmann[1], S. M. Andrievsky[2,3], I. Egorova[3,4], G. Hildebrandt[5], S. A. Korotin[3,4], K. P. Panov[6], G. Scholz[5], and D. Schönberner[5]

[1] Thüringer Landessternwarte Tautenburg, Karl-Schwarzschild-Observatorium, 07778 Tautenburg, Germany
[2] Instituto Astronômico e Geofísico, Universidade de São Paulo, Av. Miguel Stefano, 4200, São Paulo SP, Brazil
e-mail: sergei@andromeda.iagusp.usp.br
[3] Department of Astronomy, Odessa State University, Shevchenko Park, 65014 Odessa, Ukraine
e-mail: scan@deneb.odessa.ua
[4] Isaac Newton Institute of Chile, Odessa Branch, Ukraine
[5] Astrophysikalisches Institut Potsdam, An der Sternwarte 16, 14482 Potsdam, Germany
e-mail: ghildebrandt@aip.de, gscholz@aip.de, deschoenberner@aip.de
[6] Institute of Astronomy, Bulgarian Academy of Sciences, Sofia, Bulgaria
e-mail: kpanov@astro.bas.bg

Received 21 May 2001 / Accepted 6 December 2001

Abstract. In the framework of a search campaign for short-term oscillations of early-type stars we analysed recently obtained spectroscopic and photometric observations of the early A-type spectroscopic binaries 21 Her and γ Gem. From the radial velocities of 21 Her we derived an improved orbital period and a distinctly smaller eccentricity in comparison with the values known up to now. Moreover, fairly convincing evidence exists for an increase of the orbital period with time. In addition to the orbital motion we find further periods in the orbital residuals. The longest period of $57\overset{\mathrm{d}}{.}7$ is most likely due to a third body which has the mass of a brown dwarf, whereas the period of $1\overset{\mathrm{d}}{.}48$ could be related to the half rotational period of the star. For the spectral types we deduced A1 III for the primary and M for the secondary. Two further periods of $0\overset{\mathrm{d}}{.}21$ and $0\overset{\mathrm{d}}{.}22$ give hint to the existence of short-term pulsations in 21 Her. Their period difference is of the order of the expected rotational period so that one possible explanation could be rotational splitting of nonradial pulsation modes. Because of the very strong aliasing of the data this finding has to be confirmed by observations having a more suitable time sampling, however. The analysis of photometric series and the Hipparcos photometry give no certain evidence for periodic light variations. For γ Gem, besides the orbital *RV* variation, no variations with amplitudes larger than about $100\,\mathrm{m\,s^{-1}}$ could be detected. The orbital elements of γ Gem are only slightly changed compared to the previously known orbital solution by including our new radial velocities, but their accuracy is improved. For some chemical elements we determined their abundances, NLTE values of C, O, and Na as well as LTE values of Mg, Sc, Fe, Cr, and Ti. We find the abundances to be rather close to the solar values, only carbon shows a little underabundance.

Key words. stars: binaries: spectroscopic – stars: individual: 21 Her, γ Gem – stars: oscillations – stars: abundances

1. Introduction

The more recent detection of short-term radial velocity changes and moving bumps in the A0 star γ CrB shows that pulsations can be present in stars of this spectral type (Lehmann et al. 1995, 1997, 1998; Scholz et al. 1998). By means of spectroscopic and photometric observations of some selected late B- and early A-type stars we search for short-term light and radial velocity changes. If the star is a binary, the basic condition to look successfully for pulsations and for possible relations of existing pulsations to the orbital motion is the accurate knowledge of the orbital elements.

We have investigated 21 Her, because its orbital parameters are only poorly known and, apart from the radial velocity changes occurring with the binary period, no other variations are noted. The study of the sharp-lined star γ Gem is concentrated on the aspect to verify the proposed short-term spectral variabilities (Scholz et al. 1997, hereinafter Paper I), and to derive the abundances of the chemical elements C and Na which are not known up to date.

Send offprint requests to: H. Lehmann,
e-mail: lehm@tls-tautenburg.de

* The research is based on spectroscopic observations made with the 2 m telescope at the Thüringer Landessternwarte Tautenburg, Germany, and photometric observations with the 0.6 m telescope of the National Astronomical Observatory Rozhen, Bulgaria.

1.1. 21 Her

21 Her (o Her, HR 6111, HD 147869, GC 22058) has been known for more than three-quarters of a century to be a radial-velocity (*RV* hereinafter) variable. The star was reported by Harper (1928) as a spectroscopic binary. From the analysis of 29 prism spectrograms he gave the following elements:

$P = 4\overset{\mathrm{d}}{.}915$, $e = 0.511$, $K = 16.28\,\mathrm{km\,s^{-1}}$, $\omega = 355.92°$, where P is the period, e the eccentricity, K the semi-amplitude, and ω the longitude of periastron. Adding 12 further spectrograms in the following years Harper (1934) proposed a second period of $5\overset{\mathrm{d}}{.}0193$ which could just as well fit the observations.

In the following decades no further efforts have been obviously made to improve Harper's orbital parameters, because in the catalogues of the orbital elements of spectroscopic binaries, e.g. Batten et al. (1989), only Harper's values are listed. Concerning light variations of 21 Her no changes related to the 5 d binary period or with any other period are known.

The spectral type listed in the literature does not match very well: Cowley et al. (1969) classified 21 Her as an A2p star whereas Abt & Morrell (1995) noted a spectral type of A1 III. On the other hand, similar values of the projected rotational velocity, $v \sin i$, have been published: Bernacca & Perinotto (1971) obtained $50\,\mathrm{km\,s^{-1}}$, Abt & Morrell (1995) $55\,\mathrm{km\,s^{-1}}$, respectively.

1.2. γ Gem

γ Gem (HR 2421, HD 47105, GC 8633) is a well known spectroscopic binary with a period of more than 10 years. More recent determinations of the orbital elements have been published by Kamper & Beardsley (1987), Fekel & Tomkin (1993), and Scholz et al. (1997). The elements derived by the last-mentioned authors are:
$P = 4614\overset{\mathrm{d}}{.}51$, $e = 0.8941$, $K = 11.90\,\mathrm{km\,s^{-1}}$, $\omega = 312.2°$.

Different statements exist about the existence of short-period *RV* variations. In the discussion on the pros and cons of the existence of Maia variables given by McNamara (1987), γ Gem is mentioned to have short-term variations. This statement resulted from radial velocity observations of the stars γ Gem, α Lyr, and θ Vir obtained by Beardsley & Zizka (1977) at the Allegheny Observatory. According to these authors the stars should have periodic velocity variations of $0\overset{\mathrm{d}}{.}13$, $0\overset{\mathrm{d}}{.}19$, and $0\overset{\mathrm{d}}{.}15$, respectively. Although short-period variations were obviously present in all the observations made at the Allegheny Observatory during the time interval between 1962 and 1974 a later effort to confirm the short-period variation of θ Vir with another telescope and spectrograph did not give any changes of the expected kind. Therefore, Wolff (1983) concluded that the periods are very probably based on an instrumental effect. Another hint at the possible existence of short-term velocity variations follows from the assumption of Davies et al. (1978) that γ Gem is a γ-ray source. According to their model a neutron star orbits γ Gem in $1\overset{\mathrm{d}}{.}5$ at a distance of a few stellar radii which implies *RV* variations of at most $70\,\mathrm{m\,s^{-1}}$. Furthermore, the central intensities of two Si II lines and the Hα line, obtained in two nights of observations at Ondřejov, seem to show slight but systematic differences indicating the presence of short-term variations (see Paper I).

Table 1. Journal of the spectroscopic and photometric observations. N_r is the number of the runs, N_n the number of the spectrograms/photometric measurements, and N_l the number of the lines measured in one spectrogram.

star	JD 2 451 000+	N_r	N_n	N_l
Spectroscopy				
21 Her	290−717	19	603	10
γ Gem	260−268	5	320	29
Photometry				
21 Her	336−739	24	499	

On the other hand, in Paper I all known *RV*s (730 values) have been analysed with regard to the presence of velocity variations on time scales of hours and weeks. The search for periods after subtracting the orbital solution was carried out within the entire data set and within individual subsets. In contrast to Beardsley & Zizka none of the data sets reveals short-period variations with amplitudes exceeding $1\,\mathrm{km\,s^{-1}}$ in the period interval from 0.01 to 30 d.

Because of the controversy about the existence of short-term velocity variations and, because the star is sometimes considered as a spectrophotometric, MKK, and rotational-velocity standard star, a reliable conclusion has to be established. However, the amplitudes of possible *RV* variations should be distinctly smaller than $1\,\mathrm{km\,s^{-1}}$. In order to set up more stringent limits on the existence of short-term variability as before we devoted some specific observational runs to this problem.

According to Paper I the projected rotational velocity of γ Gem is $10\,\mathrm{km\,s^{-1}}$ what allows us to determine not only very precise *RV*s but also reliable elemental abundances. Because previous investigations do not give abundances for the elements C and Na we have chosen 30 spectrograms of our observational set for the determination of the abundances, especially of these but also of several other elements.

2. Observations and reductions

2.1. Spectroscopy

In March, April, and May 1999 and in May and June 2000 we obtained several series of CCD spectrograms of 21 Her and γ Gem with the coudé échelle spectrograph of the 2 m telescope of the Thüringer Landessternwarte Tautenburg (hereinafter TLS). The logs of the observations are summarized in Table 1. Throughout, the time sampling was 5 min, allowing 4-min exposures for each spectrogram. The spectrograms have a two-pixel resolution of 37 000 and a mean S/N ratio $\gtrsim 300$.

Table 2. Orbital elements of 21 Her. Solution I from Harper's *RV*s; II from the TLS *RV*s; III from the combined weighted data sets including a variable orbital period; IV final solution after subtracing the found four additional variations with periods P_i and half-amplitudes K_i. The error of the last two digits of the orbital elements is given in parenthesis.

		solution I	solution II	solution III	solution IV	P_i [d]	K_i [km s^{-1}]
P	d	5.01977(13)	5.020088(44)	5.020085(43)	5.019928(28)		
dP/dt	sec y^{-1}	–	–	0.546(56)	0.343(37)		
K	km s^{-1}	15.1(1.9)	14.712(31)	14.744(31)	14.831(20)		
e		0.519(74)	0.2056(26)	0.2060(26)	0.2091(16)	$P_1 = 57.67(2.2)$	0.58
T		2421199.99(16)	2451187.8935(76)	2451187.8930(76)	2451187.9104(49)	$P_2 = 1.4822(14)$	0.51
ω	deg	346.0(94)	15.57(62)	15.55(63)	16.13(40)	$P_3 = 0.210599(29)$	0.17
$\gamma_{\rm Harper}$	km s^{-1}	−33.10(89)	–	−32.47(97)	−32.55(94)	$P_4 = 0.223824(33)$	0.16
rms$_{\rm Harper}$	km s^{-1}	4.79	–	5.46	5.30		
$\gamma_{\rm TLS}$	km s^{-1}	–	−30.437(26)	−30.507(25)	−30.578(16)		
rms$_{\rm TLS}$	km s^{-1}	–	0.52	0.48	0.31		

All spectrograms were reduced with a modified MIDAS procedure developed by one of us (H.L.). Wavelength calibration was done using a Th-Ar lamp, and the *RV* zero point was calibrated by a large set of telluric lines in the Hα region for each spectrum separately. The Hα and Hβ profiles were fitted by a combination of cauchy and Gaussian functions. A special computer program disentangled the telluric H_2O lines from the wings of the broad Hα line profile. The line positions of metal lines have been determined by Gaussian fits and all *RV*s correspond to the line centroids and not to the line minima.

*RV*s of 21 Her were determined from Hα, Hβ, and 8 metal lines of Fe I, Fe II, and Mg I and then averaged. The *RV*s of γ Gem are the mean values taken from the different ions of 29 metal lines of Fe I, Fe II, Mg I, and Si II. All lines are lying between Hα and Hβ.

2.2. Photometry

To study the photometric behaviour of 21 Her we have observed the star with the 60 cm photometric telescope of the Rozhen National Astronomical Observatory. As comparison star we used HD 149121. The computer controlled photometer is equipped with an EMI 9789QB multiplier, a set of u, b, v filters and a diaphragm of 28″. The reduction includes corrections for dead-time and background, differential extinction and transformation to the standard UBV system. Moreover, we checked also the data of the Hipparcos photometry for variability. The logs of the photometric observations are also summarized in Table 1.

2.3. Data analysis and period search

For the determination of the orbital elements of 21 Her we use the method of iterative differential corrections (Schlesinger 1908; Sterne 1941). The method has the advantage of iterating the orbital period together with the orbital elements. Our program extends the algoritm to allow also for a calculation of apsidal motion and/or a linear decrease or increase of the orbital period.

To search for periodicities differing from the orbital period we subtract the orbital solution from the data and calculate a modified Scargle diagram of the residuals. The ordinate of the periodograms is based on the reduction in the sum of squares, it is $S = 1 - \sigma_{\rm r}^2/\sigma_0^2$, where $\sigma_{\rm r}^2$ is the variance of the residual of the sinewave fit and σ_0^2 is the total variance of the data. For the representation of the periodograms (Figs. 1, 5, 6) the number of frequency points was reduced to about 7000 by omitting local minima. A description of the period search method has been given by Lehmann et al. (1999). In the case of multiperiodicity we use a program which optimizes several periods simultaneously by a least squares fit of sinewaves. The mutual subtraction of the orbital solution and of the short-term multiple frequencies found from the measured *RV*s is done iteratively until convergency is achieved.

3. 21 Her

3.1. Orbital variations

In Table 2 we summarize our results for the orbital parameters. Solution I gives the elements calculated for the *RV*s of Harper (1928, 1934), which agree quite well with the elements determined by himself (see Sect. 1.1). Solution II lists the orbital elements following from the TLS *RV*s. Comparing with the values derived from Harper's *RV*s we get a distinctly lower eccentricity from 0.21 against 0.52 and a difference in the orbital period of 27 s. The longitude of periastron ω differs significantly with it.

Imposing the orbital period of solution II to Harper's *RV*s leads to a phase shift of about 0.5 between the TLS and Harper's data sets. There may be several reasons for this. On the one hand, the time basis of the TLS data is too small to derive a period relation which is accurate enough to link also the older data sets. On the other hand, we can not exclude apsidal motion and/or orbital period changes. To check this the orbital elements were calculated by using both Harper's and the TLS *RV*s and applying a strong weighting scheme. The *RV*s are weighted according to the observed rms of the residuals of the orbital solutions I and II. According to these values Harper's *RV*s got

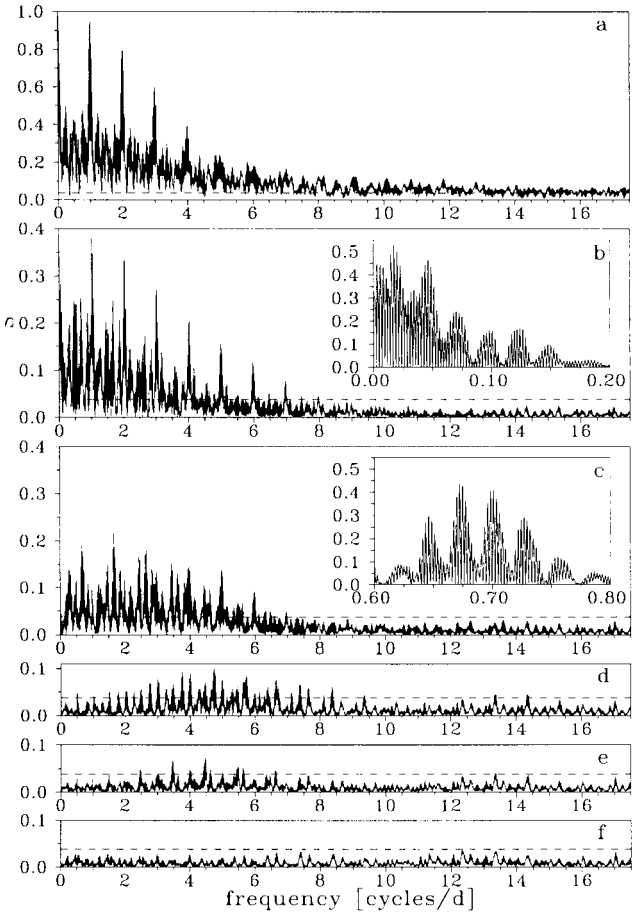

Fig. 1. Window function and periodograms of the TLS *RV*s of 21 Her at various steps of succsessive pre-whitening. **a)** Window function; **b)** only orbital solution III subtracted; **c)** pre-whitened for P_1 (largest peak at the 1 d alias of P_2); **d)** pre-whitened for P_1 and P_2 (largest peak at P_3); **e)** pre-whitened for P_1 to P_3 (largest peak at P_4); **f)** residuals. The two cut-outs in **b)** and **c)** show the regions of the P_1 and P_2 peaks, respectively, after the final optimization. The dashed horizontal lines mark the 1% FAP limit.

a weight of one hundred times smaller than those of the TLS *RV*s. The resulting elements are given in solution III of Table 2. We obtain a slight increase of the orbital period of about 0.5 s per year which corresponds to a mean difference between Harper's and the TLS observations of about 36 s. The calculated contribution of apsidal motion is not significant, however. It is remarkable that the rms of the residuals of the TLS data derived from the combined solution is lower than for solution II which was calculated only from the TLS *RV*s itself. So the derived increase in the period links not only sufficiently both data sets but gives also a better fit of the TLS data alone.

3.2. Variability on other time scales and the final orbital solution

To search for further periods we use only the TLS *RV*s and subtract orbital solution III. The window function of the data is completely dominated by the 1 d alias peaks

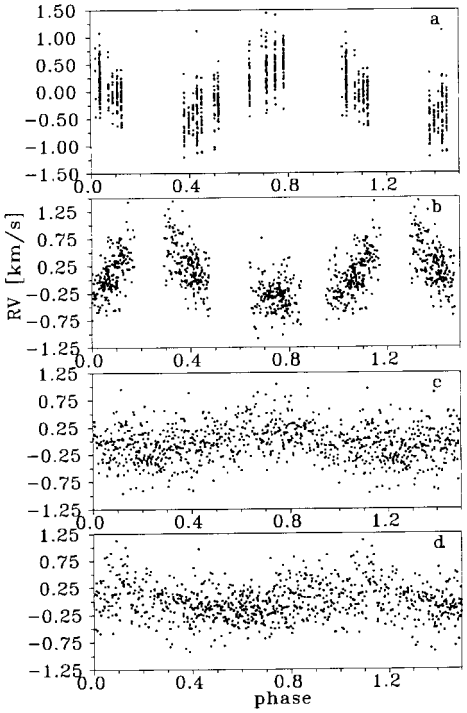

Fig. 2. Phase diagrams of the orbital residuals of 21 Her folded with the periods P_1 to P_4 **a)** to **d)**, respectively).

(Fig. 1a). The highest peak in the periodogram of the residuals (Fig. 1b) corresponds to a period of $P_1 = 58$ d. This period shows the most convenient phase diagram (Fig. 2a). The average slope inside each data group corresponds to the slope as it is expected from a sinusoidal behaviour. Moreover, this period minimizes the height of all peaks after pre-whitening. In the residuals, the highest peak corresponds to $0\overset{\mathrm{d}}{.}60$ (Fig. 1c) which is a 1 d alias of $P_2 = 1\overset{\mathrm{d}}{.}49$, the period corresponding to the second highest peak. A two-dimensional period search confirms the values found for P_1 and P_2 as the best fit. Moreover, if we subtract one of the contributions found from the two-period optimization and calculate the periodogram of the residuals, the height of the P_1 and P_2 peaks increases remarkably (cut-outs in Figs. 1b, c).

Next we find the two short-term variations P_3 and P_4 with periods near to $0\overset{\mathrm{d}}{.}21$ and $0\overset{\mathrm{d}}{.}22$ (Figs. 1d, e). After the multiple frequency optimization of all periods found we subtract our four-frequency model from the measured *RV*s, calculate a corrected orbit and repeat the entire procedure. No further periodicity can be found in the periodogram of the residuals of the final solution since all peaks are below the calculated limit of 0.038 for a 1% false alarm probability (Fig. 1f). For this check we calculated an empirical false alarm probability (FAP[1]) distribution (Fig. 3) by a large number of synthetic data sets, in the same way as described in Lehmann et al. (1999).

[1] FAP(S) describes the probability of the occurrence of a peak of the height S or higher in a periodogram obtained from data which contain only noise.

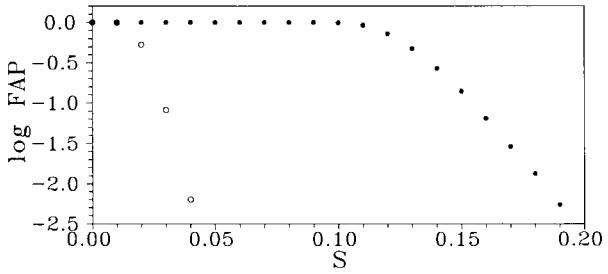

Fig. 3. Empirical false alarm probability distributions for the TLS *RV*s (open circles) and the Hipparcos data (dots) of 21 Her. The diagram shows the FAP versus peak height S.

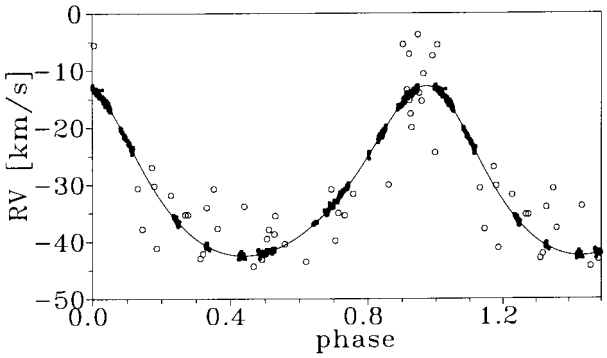

Fig. 4. Orbital solution IV of 21 Her. Harper's *RV*s are given by open circles and the TLS *RV*s by dots.

Table 2 lists the final orbital elements (solution IV) and the values of P_1 to P_4. For every period, the error is estimated from the HWHM of the fully resolved frequency peaks in the periodogram which arise from the 1 year aliasing. A typical HWHM-value is 0.00065 c d^{-1}. Furthermore we checked any combination of alias peaks neighboured to the strongest peaks in our multiple frequency search to be sure that the solution derived from the strongest peaks minimizes the total rms of the residuals.

The two short-term periods of $0\overset{\mathrm{d}}{.}21$ and $0\overset{\mathrm{d}}{.}22$ should be considered with care. Although the height of the peaks in the periodograms of both periods are far above the 1% FAP limit, the deduction of these periodograms was not straightforward in the sense of successive pre-whitening of the data. Due to the fact of strong aliasing we could not choose in every case the highest peak in the periodogram for further pre-whitening but we had to choose the peak which reduces all alias peaks to the most amount. We have checked, however, that only the four frequencies included in our final solution IV lead to the clean periodogram of the residuals which includes no further significant peaks. All other solutions (e.g. taking the 1 d alias peak of P_2 which is the strongest peak in the corresponding periodogram instead of P_2) let us find a clean periodogram of the final residuals only after much more steps of pre-whitening.

For the TLS *RV*s the rms of the residuals is reduced to 0.31 km s^{-1}. The phase diagrams of P_1 to P_4 are shown in Fig. 2, the final orbital solution in Fig. 4.

3.3. Photometric behaviour

Table 3 lists some photometric observational data of the Hipparcos and Rozhen photometry of 21 Her and the comparison star HD 149121. Figure 5 shows the window function and the periodogram of the Rozhen photometry. Both are completely dominated by the 1 d alias peaks which prevents us to determine any periodic signal. The Rozhen data are shown in Fig. 7a folded with the orbital period of 21 Her.

In Fig. 6a we show the window function of the Hipparcos data. An effective Nyquist frequency of about 34 cycles d^{-1} can be deduced and all the other periodograms in Fig. 6 have been developed up to this

Table 3. Hipparcos and Rozhen photometry of 21 Her and the comparison star. HIP is the Hipparcos catalogue number, N_{HIP} the number of measurements included in the catalogue, and H_{P} denotes the mean brightness in the Hipparcos photometric system. rms_1 is the mean error per single measurement, rms_3 is the mean error of the magnitude difference HD 149121 − 21 Her per single measurement, and rms_2 and rms_4 are the averaged deviations from the mean values of the time series.

star	21 Her	HD 149121	
Hipparcos			
HIP	80351	81007	
N_{HIP}	149	162	
JD 2 440 000+	7907–9031	7908–9063	
H_{P}	5.8468	5.6204	mag
rms_1	5.8	5.4	mmag
rms_2	2.9	1.6	mmag
Rozhen			
rms_3	7.3		mmag
rms_4	7.2		mmag

frequency. The highest peak in Fig. 6c correponds to a period of $0\overset{\mathrm{d}}{.}0835157$. There is some doubt on the existence of this period, however. The height of the peak is below the 5% FAP level (Figs. 3, 6c). Moreover, it can be an alias of a peak at lower frequency corresponding to $1\overset{\mathrm{d}}{.}4924 \pm 0.0014$ which is introduced by the strong peak of the window function at about 11 cycles d^{-1} (Fig. 6b). If we subtract one of the periods ($0\overset{\mathrm{d}}{.}0835$ or $1\overset{\mathrm{d}}{.}4924$ and vice versa) the corresponding other period vanishes as well. The height of the individual peaks of the residuals are below a FAP of 50% (Fig. 6d). Although $1\overset{\mathrm{d}}{.}4924$ is close to the $1\overset{\mathrm{d}}{.}4822$ period found from spectroscopy, it does not coincide with this frequency as it can be seen from the derived errors. The errors were again derived from the HWHM of the frequency peaks. Figure 7b shows the phase diagram of the Hipparcos data folded with the $1\overset{\mathrm{d}}{.}4924$ period.

3.4. Spectral type

We use the program SPECTRUM of Gray (2001) to estimate $v \sin i$ from the metal lines and T_{eff} and $\log g$ of 21 Her by means of the Hα profile. From the 8 metal lines already used for the *RV* determination we get

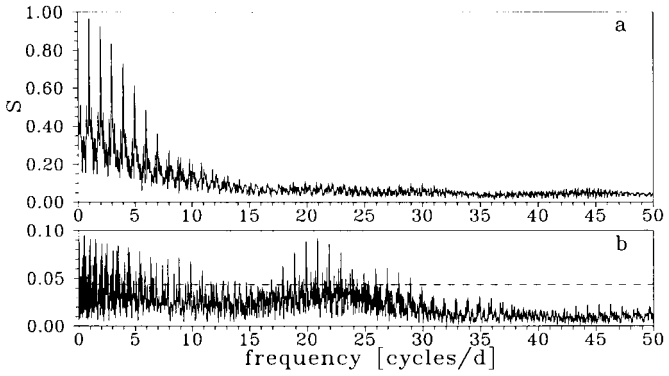

Fig. 5. Window function **a)** and periodogram **b)** of the Rozhen photometry of 21 Her. The dashed line markes the 5% FAP limit.

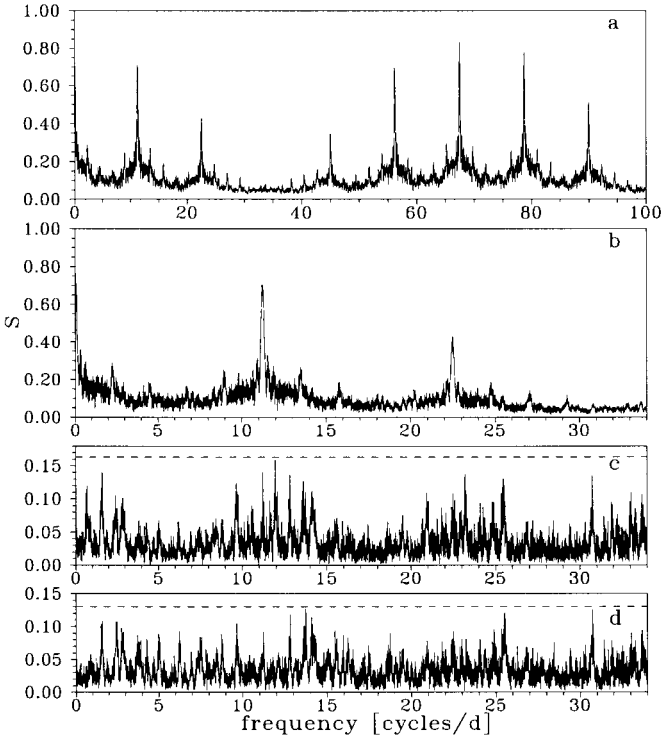

Fig. 6. Window function and periodograms of the Hipparcos photometry of 21 Her. **a)** Window function on extended scale, **b)** window function up to the Nyquist frequency, **c)** periodogram of the Hipparcos data (dashed line = 5% FAP level), and **d)** periodogram of the residuals after subtracting the $1\overset{\mathrm{d}}{.}48$ period (dashed line = 50% FAP level).

$v \sin i = 60 \pm 4\,\mathrm{km\,s^{-1}}$, close to Abt & Morrell's (1995) value of $55\,\mathrm{km\,s^{-1}}$. For Hα the best fit with a Kurucz atmosphere of solar abundances is obtained for $T_{\mathrm{eff}} = 9500\,\mathrm{K}$ and $\log g = 3.5$. Figure 8 shows the Hα profile and three line profiles calculated with different values of $\log g$.

Despite the relatively coarse steps used in both parameters ($\triangle T_{\mathrm{eff}} = 500\,\mathrm{K}$ and $\triangle \log g = 0.5$) we can assume that 21 Her is an evolved star and not a main sequence star as noted by Cowley et al. (1969).

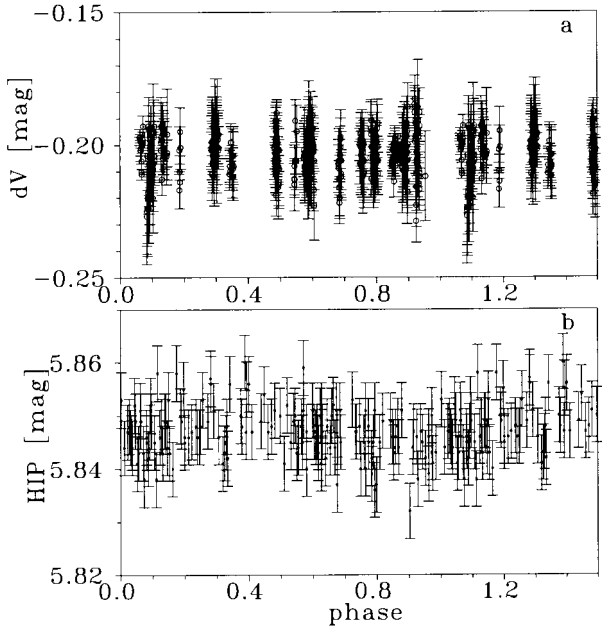

Fig. 7. Phase diagrams for 21 Her. **a)** Differential V magnitude of the Rozhen photometry folded with the orbital period, **b)** Hipparcos brightness folded with the $1\overset{\mathrm{d}}{.}4924$ period.

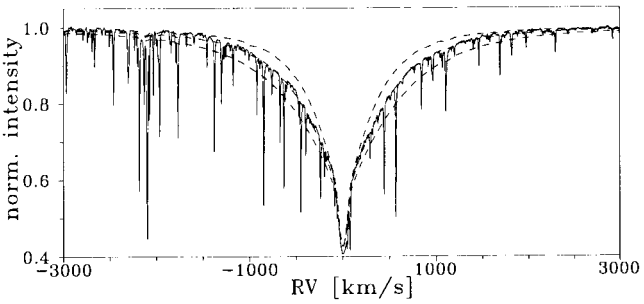

Fig. 8. Observed Hα profile of 21 Her and the line profiles (dashed lines) calculated for $T_{\mathrm{eff}} = 9500\,\mathrm{K}$ and $\log g = 3.5$ (line which fits the observed profile), $\log g = 4.0$ (broad profile), and $\log g = 3.0$ (narrow profile).

4. γ Gem

4.1. Search for short-term variations

Table 4 gives the summary of our measurements of 24 Fe I and Fe II, 3 Mg I, and 2 Si II lines. For the calculation of the mean error in RV per spectrum, $\triangle RV$, the scatter of the RVs of individual lines of a given element was first determined for every spectrum of the time series separately. Afterwards, these values were averaged over all spectra. The mean error of measurement $\triangle RV_{\mathrm{meas}}$ was derived by averaging all individual errors following from the Gaussian fits of the line center determination.

As Table 4 shows the scatter of the iron RVs is far below the error of measurement. Hence, the iron RVs derived from the 320 spectrograms are constant within the limits of the measuring accuracy. The larger deviations for the Mg I and Si II lines can be explained by weak blends in the magnesium lines and by the clearly visible telluric

Table 4. *RV*s of γ Gem and errors in km s^{-1} measured for the metal lines. <*RV*> is the mean *RV* and its error derived from the N lines and from all spectra. $\triangle RV$ is the mean deviation per spectrum and $\triangle RV_{\rm meas}$ is the mean error of measurement (see also the explanation in 4.1). Fe stands for the mean of Fe I and Fe II.

element	N	<*RV*>	$\triangle RV$	$\triangle RV_{\rm meas}$
Fe I	14	-13.996 ± 0.004	± 0.072	± 0.142
Fe II	10	-13.997 ± 0.006	± 0.107	± 0.131
Fe	24	-13.996 ± 0.003	± 0.054	± 0.094
Mg I	3	-13.784 ± 0.020	± 0.358	± 0.140
Si II	2	-14.230 ± 0.037	± 0.662	± 0.188

Table 5. Orbital elements of γ Gem. (a) is derived for the data set including the new (320) *RV*s and the old (208) *RV* values of Paper I. (b) is determined from the old *RV*s alone.

	(a)	(b)		
P	4614.51	4614.51	d	(fixed)
K_1	11.881 ± 0.068	11.90 ± 0.17	km s^{-1}	
γ	-12.629 ± 0.017	-11.74 ± 0.13	km s^{-1}	
e	0.8933 ± 0.0013	0.8941 ± 0.0035		
T	2443999.13 ± 0.77	2443996.95 ± 0.77		
ω	312.60 ± 0.60	312.2 ± 1.4	deg	
rms	0.39	0.92	km s^{-1}	

contributions in the silicon doublet. For this reason we excluded the *RV*s derived from these lines from further investigations. Furthermore, we remind that the result of our period search in the Hipparcos photometry of γ Gem (see Paper I) gives no significant variation exceeding the rms of 3 mmag.

4.2. New orbital elements

For the recalculation of γ Gem's orbital elements we first compare the iron *RV*s of Table 4, -13.996 km s^{-1}, with the *RV*s following from the orbital solution of Paper I which distinguishs between several solutions based on different data sets. From Paper I we choose solution 4 which shows minimum scatter. With the binary period of $4614\overset{\rm d}{.}51$ the orbital phase of our new CCD spectrograms is 0.58, and the corresponding *RV* is -13.05 km s^{-1}. Thus, the new CCD *RV*s are about 1 km s^{-1} below the expected one.

In order to improve the orbital elements we combine the *RV*s used for the derivation of solution 4 of Paper I with our *RV*s determined from the Fe lines. Weights were adopted according to the weighting scheme given in Paper I. Fixing the period of solution 4 we get the new orbital solution listed in Table 5a and shown in Fig. 9. This new orbital solution should be compared with solution 4 of Paper I, which is given in Table 5b. One can see that the orbital elements are only marginally changed but the accuracy is evidently improved.

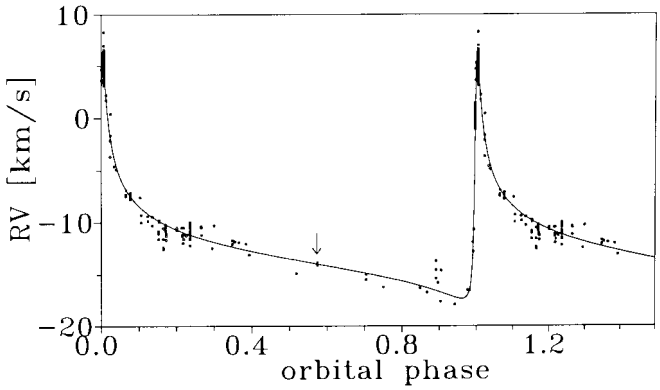

Fig. 9. Radial velocity curve of γ Gem corresponding to the new orbital solution based on the iron lines. The arrow indicates the phase of the 320 CCD *RV*s of this work.

4.3. Elemental abundances of γ Gem

Elemental abundances of γ Gem were recently derived by Hill & Landstreet (1993), Nishimura & Sadakane (1994) and Adelman & Philip (1996) using spectrograms obtained in the blue wavelength region. In all cases the abundances agree quite well with each other and are close to solar ones. To give also abundances for the elements C and Na as well as to compare the values for the other elements with those of the above-mentioned authors we used 30 TLS spectrograms for an elemental analysis. We analyzed lines of the elements C, O, Na, Mg, Si, Sc, Ti, Cr, and Fe. For the elements C, O, and Na we were able to determine the abundances by using detailed NLTE calculations which provide usually more reliable results than LTE calculations. Unfortunately, we do not have a computer code at our disposal to calculate NLTE abundances for the elements with a higher atomic number.

According to Code et al. (1976) γ Gem's effective temperature, $T_{\rm eff}$, and surface gravity, g, were found to be 9260 ± 310 K and $10^{3.6}$ (in cgs units), respectively. Recently, Napiwotzki et al. (1993) obtained 9180 and 9110 K (accuracy about 0.5 %), using Strömgren photometry, and $\log g = 3.49$ by fitting the Hγ line profile.

4.3.1. LTE calculations

The SYNSPEC spectrum synthesis (Hubeny et al. 1994) and Kurucz's (1995) Atlas9 model atmospheres have been used to derive the LTE elemental abundances. Atmospheric models were interpolated from Kurucz's grid, and oscillator strengths of the lines were taken from the catalogue of Hirata & Horaguchi (1994). According to the quality of the spectrograms the abundance calculations include different number of lines of the elements Mg I (1), Si II (2), Sc II (1), Ti II (3/6), Cr II (6/11), Fe I (8/14), and Fe II (9/13). The numbers in the brackets denote the minimal and maximal number of lines used per spectrum.

To evaluate the stellar parameters from our spectrograms, we proceeded as described in Kovtyukh & Andrievsky (1999): the effective temperature, $T_{\rm eff}$, was

Table 6. Wavelengths, oscillator strengths, and equivalent widths of the C, O, and Na lines.

Ion	λ (Å)	$\log gf$	W_λ (mean) (mÅ)
C I	5052.122	−1.24	38.0 ± 0.35
	5380.242	−1.57	19.2 ± 0.28
	7113.130	−0.76	27.0 ± 0.43
O I	6155.990	−0.67	39.2 ± 0.22
	6156.780	−0.45	55.1 ± 0.32
	6158.190	−0.31	69.9 ± 0.31
Na I	5889.953	+0.13	168.2 ± 0.84
	5895.923	−0.17	140.2 ± 0.61

determined from Fe I by demanding independence of the individual abundances on the line excitation potentials, the microturbulence velocity, v_t, by demanding independence of the individual abundances on the line equivalent widths, and the gravity, g, from the Fe I-Fe II ionization equilibrium. The Fe I excitation gave $T_\mathrm{eff} = 9100 \pm 200$ K, and from our 30 TLS spectrograms we got as means $\log g = 3.74 \pm 0.06(1\sigma)$ and $v_\mathrm{t} = 1.7 \pm 0.1(1\sigma)\,\mathrm{km\,s^{-1}}$. Our "spectroscopic" gravity is somewhat larger than that derived from the Balmer line match (see Napiwotzki et al. 1993), but we kept it for consistency.

4.3.2. NLTE calculations

The NLTE abundances of C, O, and Na were found with the help of a modified version of the MULTI code of Carlsson (1986) described in Korotin et al. (1999a) and Korotin et al. (1999b). A simultaneous solution of the radiative transfer and statistical equilibrium equations has been performed in the approximation of the complete frequency redistribution for all the lines.

The carbon atomic model consists of 115 levels: 94 levels of C I, 20 levels of C II and the ground state of the C III. The radiative transitions between the first 47 levels of C I and the ground level of C II were considered. Transitions between the remaining levels were used only in the equations of particle number conservation. 113 transitions were included in the linearization procedure, and 155 transitions were treated as those having fixed radiative rates.

The oxygen atomic model consists of 75 levels: 72 levels of O I, 3 levels of O II, and the ground state of O III. The radiative transitions between the first 23 levels of O I and the ground level of O II were considered.

The adopted sodium model (see Korotin & Mishenina 1999) consists of 27 levels of Na I and the ground level of Na II. The radiative transitions between the first 20 levels of Na I and the ground state of Na II were considered. Finally, 66 transitions were included in the linearization procedure. For 24 transitions the radiative rates were fixed. The calculation were based on the Kurucz's grid of atmospheric models.

In Table 6 we give the wavelengths of the C, O, and Na lines used, their oscillator strengths gf and the measured equivalent widths W_λ and their errors (in mÅ) for the NLTE calculations. The equivalent widths are the mean values of the 30 spectrograms and their errors correspond to the rms of these mean values.

Table 7. Mean abundances $\log$ (El/H) of γ Gem. Available error estimates are given between parenthesis in units of the last decimal.

Ion	NLTE	LTE	A&P [1]	Sun [2]
C I	−3.84(9)			−3.45
O I	−3.13(9)		−3.08	−3.13
Na I	−5.45(9)			−5.67
Mg I		−4.64	−4.28	−4.42
Si II		−4.57	−4.39(13)	−4.45
Sc II		−9.14	−9.08(25)	−8.83
Ti II		−6.98(8)	−6.83(26)	−6.98
Cr II		−6.25(9)	−5.93(26)	−6.33
Fe I		−4.45(10)	−4.36(18)	−4.50
Fe II		−4.46(7)	−4.37(18)	−4.50

[1] Abundances from Adelman & Philip (1996).
[2] Solar abundances are those recommended by Grevesse et al. (1996).

4.3.3. Results

In Table 7 we compare our abundances with those of Adelman & Philip (1996) and with solar values given by Grevesse et al. (1996). Error estimates are given when available.

To estimate the accuracy of our values we consider the element iron. A significant dependence between abundances from individual iron lines and excitation potentials of their lower level appears when the temperature is changed by more than 200 K. This value can be assumed as the error of the T_eff determination. For the estimation of the uncertainty of the iron abundance we presuppose a variation of T_eff by ±200 K, $\log g$ by ±0.06, and v_t by $\pm 0.1\ \mathrm{km\,s^{-1}}$(cf. Sect. 4.3.1) resulting in iron abundance changes of respectively 0.10 and 0.07 dex for Fe I and Fe II. Therefore, no disagreement between both analyses can be established. For the other elements, only one ion and few spectral lines were available. So we can give for these elements only the rms derived from the 30 spectrograms. The abundances derived for Mg, Si, and Sc are based on only one or two spectral lines, therefore we can not estimate its accuracy.

Adelman & Philip's values are based on the atmospheric parameters $T_\mathrm{eff} = 9260$ K, $\log g = 3.6$, and $v_\mathrm{t} = 2.0\,\mathrm{km\,s^{-1}}$ given already by Code et al. (1976). Their abundances seem to be slightly larger than in our analysis. But, apart from a slight adjustment occurring from the small differences in the adopted atmospheric parameters, the present differences of both analyses are still included in the range of the errors.

The derived abundances are close to solar, only the element C could be somewhat depleted.

Table 8. Masses of the second and third component and semi-major axes of the corresponding orbits derived for two different orbital inclinations i and assuming a mass of the primary of $4\,M_\odot$.

i	M_2 $[M_\odot]$	$a_{1,2}$ $[R_\odot]$	M_3 $[M_\odot]$	$a_{(1,2),3}$ $[R_\odot]$
90°	0.31	20.1	0.03	102
45°	0.45	20.3	0.04	104

5. Discussion

21 Her. From the new *RV*s of 21 Her we determined an essentially improved orbital solution. Besides the derivation of a more precise orbital period we could show that the eccentricity of the orbit is less than half of the value adopted so far, and that the system shows a mean increase of the orbital period of $0.34\,\mathrm{s\,yr^{-1}}$. Applying this value to the epoch difference between Harper's and our *RV*s we got a period difference of about 25 s which is in a very good agreement with the period difference of 27 s following from the separate orbital solutions.

In addition to the orbital *RV* variation we found four further periods. Concerning the origin of the two longer periods we can only make some speculations. The period P_1 of nearly 58 d is on a time scale which we can assign only to the presence of a third body in the 21 Her system. The period P_2 of 1.48 d could be related to the rotational time scale. Presupposing these conclusions are correct we can make some estimations on the configuration of the system 21 Her.

Assuming $P_{\mathrm{rot}} = 2\,P_2$ it follows, together with the observed $v \sin i$ of $60\,\mathrm{km\,s^{-1}}$ a lower limit of the stellar radius of $3.5\,R_\odot$. From the mass function

$$M_2^3 = 1.036 \times 10^{-7}\,\frac{K_1^3 P_{\mathrm{orb}}}{\sin^3 i}\,(1-e^2)^{3/2}\,(M_1+M_2)^2 \qquad (1)$$

we get lower limits of the mass of the secondary M_2 and, together with the third Keplerian law, of the semi-major axis $a_{1,2}$. In this way we can also estimate the mass M_3 and the orbital diameter $a_{(1,2),3}$ of the hypothetical third body, supposing the system consists of a central mass of $M_1 + M_2$ which is revolved by M_3. Table 8 gives values calculated for $M_1 = 4\,M_\odot$, corresponding to the stellar parameters of an A0 III primary as tabulated by Schmidt-Kaler (1981), and for orbital inclinations of 90° and of 45°. The inclination of 90° gives lower limits of all values. The other inclination follows from the observed $v \sin i$ if we assume a rotational period of 3 d, an A0 III star radius of $R_1 = 5\,R_\odot$, and coplanarity between the rotational and orbital axis. The results show, independent of the orbital inclination, that the secondary is of very late spectral type in the range of the M stars and that the third body must be a brown dwarf. From the parallax of 21 Her of 9.6 mas as measured by the Hipparcos satellite we can estimate the maximum angular separation of the third body to be of about 5 mas.

If the two frequencies P_3 and P_4 are real we have to explain the observed frequency splitting. The frequency difference corresponds to a period of about 3.5 d which is again in the order of the rotational period of the primary as expected so far. In this case the two variations itself could be interpreted as rotational splitted nrp modes if we assume that both pulsations have the same degree l and a difference $\triangle m = 1$ in azimuthal number. From $v \sin i$ we get a lower limit of the radius of 21 Her of $4.2\,R_\odot$. This estimation as well as that of $3.5\,R_\odot$ mentioned above for the P_2 variation is compatible with $\log g = 3.5$ which follows from the best Hα profile fit and is also in agreement with the classification of 21 Her as an A1 III star given by Abt & Morrell (1995).

The period search based on the Hipparcos data shows the strongest peak at a period of $0\overset{\mathrm{d}}{.}0835$. This period could be an alias introduced by the time sampling of the Hipparcos satellite. Then the correct period of $1\overset{\mathrm{d}}{.}49$ is near to the $1\overset{\mathrm{d}}{.}48$ period found from radial velocities. Because of the relatively high FAP of about 7% of the found peak we consider this detection as marginal, however, and mention it only as worthy for a check by further photometric investigations.

γ Gem. The measured *RV*s of γ Gem are constant over the time interval of 8 d covered by our observations. From the errors listed in Table 4 one can immediately conclude that it is not possible to find any short-term periods. In the Scargle diagram we found indeed only peaks at the 1 d aliases at 1 d, 1/2 d, up to 1/6 d. Thus, in our series no *RV* variations with amplitudes larger than about $100\,\mathrm{m\,s^{-1}}$ are present, and it is impossible to detect the small *RV* changes expected by Davies et al. (1978) based on the assumption that γ Gem is revolved by a neutron star. The hint at the existence of very weak variations of the central intensities of Hα and Si II lines, mentioned in Paper I, is very probably produced by variable contributions of telluric lines.

In Paper I the extraordinary long orbital period of γ Gem was determined from a set of more than 700 *RV*s. Due to the position of our new *RV*s in the orbital phase it is not possible to improve the period. Because our observations give very precise *RV*s, however, we have examined the agreement between the recently derived CCD *RV*s and the *RV*s following from solution 4 of Paper I. According to our earlier investigation (Paper I), a slight increase of the γ-velocity with time seems to be indicated. Comparing the γ-velocities in Table 5 we find, including our new *RV*s into the orbital calculation, a smaller γ-velocity, however. So we think, considering the quite different quality of the individual data sets used for the analysis of the binary behaviour in the past, that the previously supposed γ-variation is very probably an artefact due to an insufficient correction of the *RV* zero points in Paper I.

On the basis of 30 TLS spectrograms we derived abundances of C, O, Na (NLTE) and Mg, Si, Sc, Ti, Cr and Fe (LTE). Considering the errors included in the abundances the values show no significant deviations to those of the sun. The only exception seems to be the element C which shows underabundance. The investigation characterize γ Gem as a normal A star.

6. Conclusions

The present investigation of 21 Her shows once more that stellar pulsations can be found in almost all regions of the H-R diagram. Our previous studies on other stars (e.g. γ CrB, γ UMi, or ET And) have proved that periodic *RV* variations with time-scales of hours occur in different types of early A stars, as peculiar stars and giants. For these stars a common characteristic is obviously their more or less evolved state. To clarify the pulsational properties, especially to disentangle the variations caused by pulsation, by rotation, and by orbital motion and also to overcome all aliasing problems, multisite observations are necessary and the use of the WET technique is desirable. This remark concerns also the confirmation of the hypothetical third body in the 21 Her system. The star should be a brown dwarf surrounding a double star consisting of an evolved A-type star and a late M-type star. Because of the very low angular separation of only 5 mas and the presence of the M star a direct observation of the brown dwarf should not be possible.

Acknowledgements. K.P. would like to thank for the hospitality during his visit to Astrophysikalisches Institut Potsdam. He acknowledges also the support by the Deutsche Forschungsgemeinschaft, 436 BUL 113-102-0, and the support by the Bulgarian National Science Foundation, grant F 826. S.M.A. would like to express his gratitude to FAPESP (Brazil) for the visiting professor fellowship No. 2000/06587-3. The authors are indebted to the referee, Dr. P. De Cat, for his comments which helped to improve the paper.

References

Abt, H. A., & Morrell, N. I. 1995, ApJS, 99, 135
Adelman, S. J., & Philip, A. G. D. 1996, MNRAS, 282, 1181
Batten, A. H., Fletcher, J. M., & MacCarthy, D. G. 1989, Publ. Dom. Astrophys. Obs., 17
Beardsley, W. R., & Zizka, E. R. 1977, Current Problems in Stellar Pulsation Instabilities, NASA Technical Memorandum 80625, 421
Bernacca, P. L., & Perinotto, M. 1971, Contr. Asiago No. 250
Carlsson, M. 1986, Uppsala Obs. Rep., 33
Code, A. D., Davis, J., Bless, R. C., et al. 1976, ApJ, 203, 417
Cowley, A., Cowley, C., Jaschek, M., et al. 1969, AJ, 74, 375
Davies, R. E., Fabian, A. C., & Pringle, J. E. 1978, Nature, 271, 634
Fekel, F. C., & Tomkin, J. 1993, AJ, 106, 1156
Gray, R. O. 2001, `www.acs.appstate.edu/dept/physics/spectrum/`
Grevesse, N., Noels, A., & Sauval, J. 1996, ASP Conf. Ser., 99, 117
Harper, W. E. 1928, Publ. Dom. Astrophys. Obs., 4, 179
Harper, W. E. 1934, Publ. Dom. Astrophys. Obs., 6, 235
Hill, G. M., & Landstreet, J. D. 1993, A&A, 276, 142
Hirata, R., & Horaguchi, T. 1994, Atomic Spectral Line List, Catalogue VI/69, CDS data base
Hubeny, I., Lanz, T., & Jeffery, C. S. 1994, Newslett. Analyses Astron. Spectra, No. 20, 30
Kamper, K. W., & Beardsley, W. R. 1987, AJ, 94, 1302
Korotin, S. A., & Mishenina, T. M. 1999, Astron. Rep., 43, 533
Korotin, S. A., Andrievsky, S. M., Kostynchuk, L. Yu., et al. 1999a, Ap&SS, 260
Korotin, S. A., Andrievsky, S. M., & Luck, R. E. 1999b, A&A, 351, 168
Kovtyukh, V. V., & Andrievsky, S. M. 1999, A&A, 351, 597
Kurucz, R. L. 1995, ASP Conf. Ser., 78, 205
Lehmann, H., Scholz, G., Hildebrandt, G., et al. 1995, A&A, 300, 783
Lehmann, H., Scholz, G., Hildebrandt, G., et al. 1997, A&A, 327, 167
Lehmann, H., Scholz, G., & Yang, S. 1998, ASP Conf. Ser., 135, 199
Lehmann, H., Scholz, G., Hildebrandt, G., et al. 1999, A&A, 351, 267
McNamara, B. J. 1987, in Lecture Notes in Physics 274, Stellar Pulsation, 92
Napiwotzki, R., Schönberner, D., & Wenske, V. 1993, A&A, 268, 653
Nishimura, M., & Sadakane, K. 1994, PASJ, 46, 349
Schlesinger, F. 1908, Publ. Allegheny Obs., 1, 35
Schmidt-Kaler, Th. 1981, Physical parameters of the stars. In Landoldt-Börnstein, Zahlenwerte und Funktionen aus Naturwissenschaften und Technik. Neue Serie, Gruppe VI: Astronomie, Astrophysik und Weltraumforschung, Band 2b (Springer-Verlag Berlin/Heidelberg/New York), 28
Scholz, G., Lehmann, H., Harmanec, P., et al. 1997, A&A, 320, 791 (Paper I)
Scholz, G., Lehmann, H., Hildebrandt, G., et al. 1998, A&A, 337, 447
Sterne, T. 1941, Proc. Nat. Acad. Sic., 27, 175
Wolff, S. C. 1983, in The A-type stars: problems and perspectives, NASA SP-463, 29